NorthStar's Fragmentation Analysis of the Intelsat 33e Breakup in GEO

Laura Pirovano
NorthStar Earth & Space
Yashica Khatri
NorthStar Earth & Space

Narendra Gollu
NorthStar Earth & Space

Matteo Budoni
NorthStar Earth & Space

Guillermo Escribano Blázquez
NorthStar Earth & Space

ABSTRACT

This paper presents NorthStar's automated orbital analysis of a satellite breakup event, demonstrating both the capabilities and limitations of current space surveillance methodologies. Multiple data providers supplied uncorrelated track (UCT) IDs associated with the fragmentation event, however proprietary constraints prevent publication of these data or disclosure of provider names. Consequently, this analysis uses simulated debris observations from the publicly available Space-Track two-line elements (TLEs) as they would appear to NorthStar space-based constellation satellites. The event provided a critical test of NorthStar's automated initial orbit determination (IOD) pipeline, which had been deployed days prior to the breakup. Twice a day, NorthStar generated comprehensive catalogued debris lists in TLE format and performed a conjunction analysis to identify potential close approaches between new debris and operational satellites. Although the automated pipeline proved essential for successful UCT handling -impossible through manual intervention alone- the event revealed critical limitations in processing borderline too-short arcs (TSAs) with predefined parameters, necessitating team intervention for successful IOD and orbit determination. These findings have directly driven NorthStar's development roadmap to enhance automated cataloguing capabilities for handling similar events while maintaining accurate catalogues essential for safe space operations.

1. INTRODUCTION

Intelsat 33E [1] experienced an anomaly on October 19, 2024 around 0430 UTC leading to a power loss followed by a fragmentation event [2], which was confirmed by Intelsat on October 21, 2024 [3]. Launched in 2016, the satellite was in a geostationary Earth orbit (GEO) orbit at a longitude of about 60 degrees at the time of the breakup. The early estimates from 19 Space Defense Squadron (SDS) of 20 tracked fragments soon grew to the order of 16,000 debris fragments greater than 1 cm in size estimated to be associated with the breakup. This number included 500 tracked fragments of size greater than 10 cm. Interestingly, the entire GEO belt longitudinal range was covered with debris pieces from the explosion within a few days. Based on European Space Agency's Debris Environment Long Term Analysis (DELTA) tool, the threat of long-term effects was limited to the GEO regime. This highlighted the very well-known issue of the catastrophe that can accompany GEO breakups and the variety of external factors that can cause such events [4].

Over several days and weeks, together with other commercial SSA Data and Service providers, and as part of its contractual engagement with the US Space Force Joint Commercial Operations [5, 6], NorthStar supported the tracking, analysis, and mitigation of the fragmentation event. One of the biggest challenges was that many new fragments were very briefly observed initially, leading to very-short arc (VSA) problems [7], and that these fragments, in many cases,

Copyright © 2025 Advanced Maui Optical and Space Surveillance Technologies Conference (AMOS) – www.amostech.com

were observed again only after long gaps. Without loss of relevance and generality regarding the used algorithm and processing frameworks described hereafter, and to comply with restricted terms of use of proprietary data involved in support of the events, presented results and figures have been re-computed from synthetic measurements. Simulated observations were generated with the NorthStar physics-based Space-based Sensor simulator. It relies on Orekit [8] and SPICE [9] to generate realistic datasets accounting for geometry and visibility constraints. The referenced historical trajectory used to seed the simulation was derived from the publicly available Space-Track [10] two-line elements (TLEs).

Once NorthStar was supplied with observations associated with the fragmentation event, NorthStar's automated pipeline proceeded with an initial orbit determination (IOD) for each newly discovered uncorrelated track (UCT). The IOD process was automatically followed by a batch least squares (BLSQ) leveraging all observations in the UCT, thus obtaining the initial guess that would be used by an extended Kalman filter (EKF) which ingested new data every 15 minutes, when available. The innovative nature of the automated IOD pipeline and the VSA nature of these tracks caused failures in the automated processes, leading to the need of manual intervention, utilising ad-hoc parameters for IODs and processing orbit determinations (ODs) using alternative methods than those in the automated pipeline to achieve improved results, which could then be used to re-initiate the pipeline. Manual work included the use of different arc lengths and observation groupings for the IODs, and alternative filters such as the adaptive robust Kalman filter (ARKF) for the ODs.

Orbital analysts could leverage NorthStar analysis to post-process the data coming from the OD pipeline to understand the distribution of the fragments in the GEO belt and the possible conjunction risks with the pre-existing GEO objects. A glimpse of our operational dashboard - the NavOps App - that contains all these tools is shown in Fig. 1. These include summaries of elements variation over time, and their accuracy, waterfall plots, neighbourhood tables, conjunction assessment tables, photometry plots, pass schedule, and relative orbit plots. The details of them are given in Section 2. All these tools together provide a comprehensive situational awareness for the GEO belt's effect from the fragmentation.

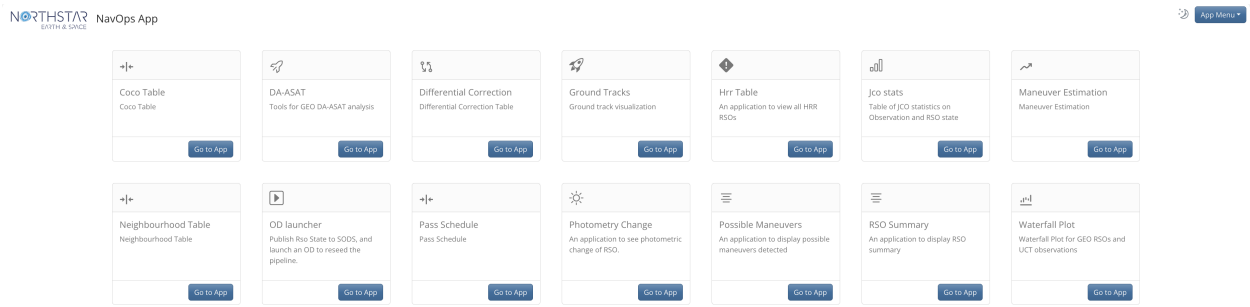

Fig. 1: NorthStar's dashboard: the NavOps App.

This paper covers the mathematical background of all the IOD and OD algorithms utilised in the automated and manual processes, showcasing the results through the situational awareness tools in Fig. 1.

2. MATHEMATICAL BACKGROUND

This section describes the main mathematical backbone of our SSA suite in Section 2.1 and presents main applications of them in Section 2.2. To help the reader navigate through the paper and understand how each input/output fit in the operational suite of tools, Fig. 2 provides a functional diagram block. The automated pipeline (Section 2.1.1) is in charge of ingesting all new UCTs, process IOD (Section 2.1.2) and OD (Section 2.1.3) to obtain refined states every time new observations of the same UCT become available. At any point within the process, an orbital analyst can manually intervene to utilise orbital analyst defined parameters and observation grouping in the IOD and BLSQ processes, and opt for different filters to obtain faster convergence on the solution. The outputs can then be used to re-seed the automated pipeline. Once updated states are available for the UCTs, different tools can be used to assess the situation:

- CAS (Section 2.2.1) - to trace back the breakup time and analyse relative geometries;

Copyright © 2025 Advanced Maui Optical and Space Surveillance Technologies Conference (AMOS) – www.amostech.com

- Neighbourhood table (Section 2.2.2) - to visualise the affected GEO area looking for possible close approaches with a specific UCT;
- Computation Of Miss Between Objects (COMBO) assessment - a collection of neighbourhood tables looking into the future and filtering for close approaches to identify potential hazards posed by a group of debris to operational satellites;
- Waterfall - to visualise the longitudinal debris spread over time in the GEO belt;
- Photometry - to assess satellites stability;
- Pass schedule - to determine the next collection opportunity for the suite of sensors available.

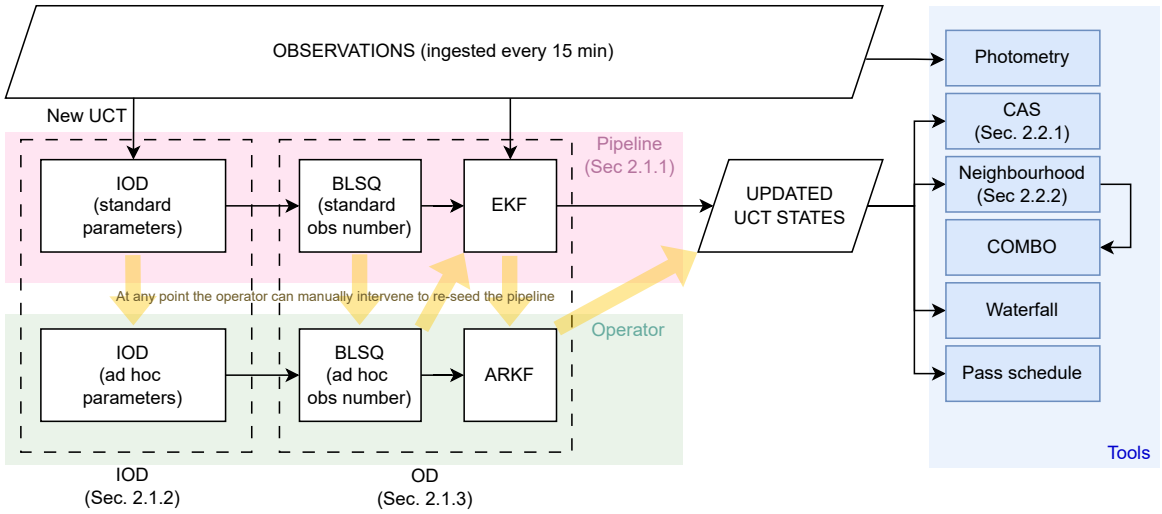

Fig. 2: Different blocks that complete SSA suite.

2.1 IOD and OD

2.1.1 Automated pipeline observations ingestion

The UCT processing starts with data ingestion in our pipeline. Fig. 3 shows the sensor data ingestion in the pipeline's Operations Center. The different coloured circles show data from different providers and the size of these circles shows the amount of observations ingested. Fig. 4 shows the processing of the observations in the Operations Center and displays the amount of valid IOD and OD jobs going through the pipeline. The not validated jobs and failed jobs relate to insufficient data and/or uncertainty of observations.

2.1.2 Initial Orbit Determination: N-Gooding Method

The purpose of IOD is to estimate an initial state with limited information availability and no a-priori information. The N-Gooding method is used to perform IODs as described in Karimi and Mortari [11] on optical observations. In this method, more than 3 angles-only observations can be leveraged to perform more accurate estimation than previously existing methods, such as Classical Gooding and Admissible Region methods. This iterative technique relies on the fact that all position vectors lie on the same plane and uses the Lagrangian coefficients (f and g). Due to the automated nature of the pipeline, arc length and number of observations were fixed, while orbital analyst intervention could leverage the full arc length and change the number of observations to be used to obtain a better initial guess. Fig. 5 shows a an example of observation collection on a UCT highlighting the N observations used for IOD.

Copyright © 2025 Advanced Maui Optical and Space Surveillance Technologies Conference (AMOS) – www.amostech.com

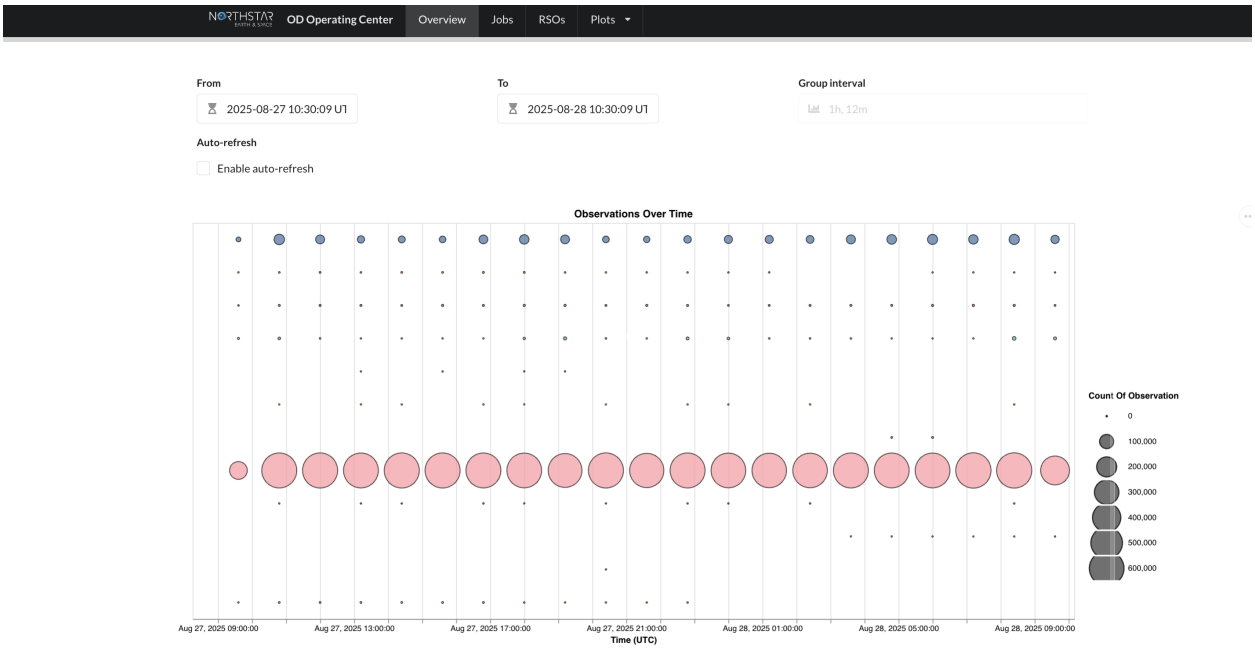

Fig. 3: Observation ingestion in Operations Center Pipeline.

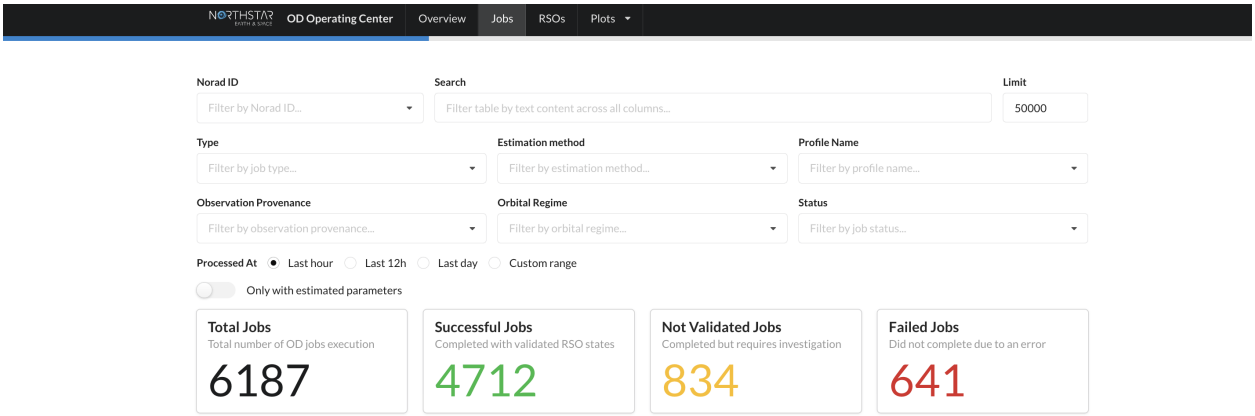

Fig. 4: Operations Center Pipeline that tracks running jobs.

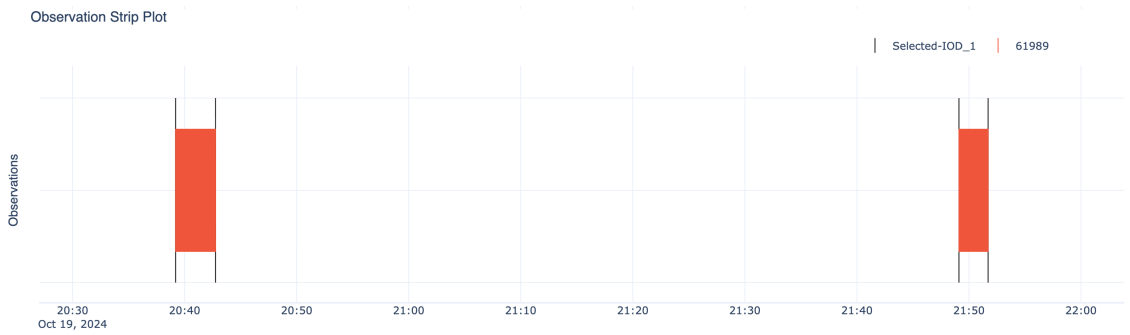

Fig. 5: Observation selection for IOD from an observation strip plot.

Copyright © 2025 Advanced Maui Optical and Space Surveillance Technologies Conference (AMOS) – www.amostech.com

2.1.3 Orbit Determination

This section describes the BLSQ, EKF and ARKF, introduced in Fig. 2. The propagation steps in each of these filtering methods use an explicit Runge-Kutta method of order 8(5,3), with the following force model: geopotential (up to order and degree 24), atmospheric drag (NRLMSISE00), solar radiation pressure, and the third-body perturbation (due to Sun and Moon).

The BLSQ refines the initial conditions (in this case the IOD solution) based on a least-squares fit on all of observations available [12], as pictured in Fig. 5. This is done iteratively while minimising the root mean square (RMS) error for the residuals between the observed and predicted measurements:

$$\min_{\mathbf{x}} \sum_{i=1}^{m} \|\mathbf{z}_i - h_i(\mathbf{x})\|^2_{\mathbf{R}_i^{-1}}$$

The EKF sequentially processes each new available track by linearising the dynamics about each observation. The filter is a two step process: prediction and update [12]. Prediction step:

$$\hat{\mathbf{x}}_{k|k-1} = f(\hat{\mathbf{x}}_{k-1|k-1}, \mathbf{u}_{k-1}) \tag{1}$$

$$\mathbf{F}_k = \left.\frac{\partial f}{\partial \mathbf{x}}\right|_{\hat{\mathbf{x}}_{k-1|k-1}} \tag{2}$$

$$\mathbf{P}_{k|k-1} = \mathbf{F}_k \mathbf{P}_{k-1|k-1} \mathbf{F}_k^\top + \mathbf{Q}_k \tag{3}$$

Where, $\mathbf{x}$ is the six dimensional state, $\mathbf{u}$ is the control input, and $\mathbf{Q}_k$ is the process noise.

Update step:

$$\mathbf{y}_k = \mathbf{z}_k - h(\hat{\mathbf{x}}_{k|k-1}) \tag{4}$$

$$\mathbf{H}_k = \left.\frac{\partial h}{\partial \mathbf{x}}\right|_{\hat{\mathbf{x}}_{k|k-1}}, \quad \mathbf{S}_k = \mathbf{H}_k \mathbf{P}_{k|k-1} \mathbf{H}_k^\top + \mathbf{R}_k, \quad \mathbf{K}_k = \mathbf{P}_{k|k-1} \mathbf{H}_k^\top \mathbf{S}_k^{-1} \tag{5}$$

$$\hat{\mathbf{x}}_{k|k} = \hat{\mathbf{x}}_{k|k-1} + \mathbf{K}_k \mathbf{y}_k, \quad \mathbf{P}_{k|k} = (\mathbf{I} - \mathbf{K}_k \mathbf{H}_k) \mathbf{P}_{k|k-1} \tag{6}$$

Where, $\mathbf{z}$ is the measurement, $\mathbf{y}$ is the residual, $\mathbf{H}$ is the Jacobian of the measurement model, $\mathbf{S}$ is the innovation covariance, and $\mathbf{K}$ is the Kalman gain. With these two steps, the EKF iteratively computes state estimates at each observation.

The ARKF is an extension of the EKF and uses an adaptive factor based on a learning statistic to handle situations such as unexpected manoeuvres or bad initial conditions where the EKF fails to converge [13]. Although the breakup fragments did not manoeuvre, ARKF was useful in achieving faster stability and robustness as new observations flowed in, given the initial conditions were obtained on VSAs. This filter was run offline, and the pipeline was re-seeded with the outputs. The adaptive factor with two regimes using a chosen threshold (c) is computed as follows:

$$\alpha_k = \begin{cases} 1, & \text{if } |\Delta X_k| \leq c \\ \frac{c}{|\Delta X_k|}, & \text{if } |\Delta X_k| > c \end{cases}$$

This adaptive factor is applied to the Kalman gain in the update step:

$$K_k = \left(\frac{1}{\alpha}\bar{\Sigma}_k H_k^T\right)\left(\frac{1}{\alpha} H_k \bar{\Sigma}_k H_k^T + R_k\right)^{-1}$$

This allows for a robust orbit update, taking into account unexpected orbit changes.

Copyright © 2025 Advanced Maui Optical and Space Surveillance Technologies Conference (AMOS) – www.amostech.com

2.2 Operations Tools

2.2.1 CAS - Conjunction Analysis System

NorthStar Conjunction Analysis System (CAS) is a software platform designed to integrate key components of conjunction analysis and collision avoidance. Its goal is to generate accurate and actionable risk assessments for upcoming conjunction events, predicted several days in advance, and to propose avoidance manoeuvres when the risk exceeds the thresholds set by the orbital analysts. By providing timely and meaningful early warnings, CAS enables the collection of additional input data and the use of advanced techniques to improve the quality of the assessment.

The platform is based on a set of software services that deliver all the required functionalities, including catalogue management, orbit and covariance propagation, conjunction screening, conjunction assessment through the computation of relevant risk key metrics such as probability of collision (PoC), miss distance, and Mahalanobis distance. These services are smoothly integrated with the collision avoidance module that enables the generation of recommended avoidance manoeuvres when needed.

One feature of CAS is widely used within NorthStar operations and proved to be very useful within the breakup event as well: that is the so-called Time, Radial, In-track, Cross-track (TRIC) plot which shows the relative position between the two resident space objects (RSOs) involved in a conjunction. Proceeding top to bottom in Fig. 6 we see:

- Four plots showing the relative position represented in norm and in the three components of the local RIC reference frame;
- the RIC components and norm evolution in time;
- a 3-dimensional relative position plot;
- the Camera Target Sun (CATS) angle over time, to help understanding the visibility conditions for the primary object over the secondary one with respect to the Sun position;
- details of the close approaches identified in terms of time of closest approach (TCA), distance of closest approach (DCA), RIC components and relative velocity.

Fig. 6: TRIC plot example.

Copyright © 2025 Advanced Maui Optical and Space Surveillance Technologies Conference (AMOS) – www.amostech.com

2.2.2 Neighbourhood Table

The NorthStar neighbourhood table is a compiled list of RSOs in proximity of a primary satellite that meet the chosen longitude, drift rate, TCA, and DCA thresholds. It uses data from both NorthStar and SpaceTrack sources to give an advanced compilation of objects in proximity. It leverages the same propagation method detailed in Section 2 to propagate the RSOs and determining time and distance of closest approach. This can be leveraged to look into the future for possible upcoming conjunctions and in the past to determine the breakup object. Fig. 7 shows the input options that are used to generate the neighbourhood table in our operations tools. A compiled list of neighbourhoods for a pool of objects with DCA within a specific threshold is called a COMBO assessment.

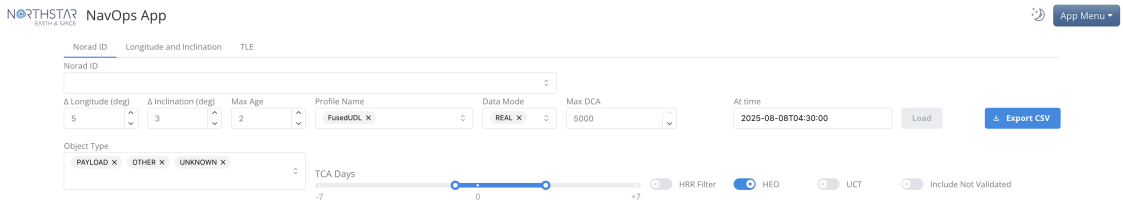

Fig. 7: Neighbourhood selection criterion.

2.2.3 Photometry

A photometric plot can be used to assess the stability of an object and to detect a tumble [14]. By plotting the visual magnitude of the object as a function of the phase angle, we get the phase function. Correcting for the brightness at visible wavelengths only, the photometric curve of the object is retrieved. This plot represents integrated brightness over all illuminated surfaces visible to the sensors (i.e. you cannot resolve for object geometry). Plotting over several days, it typically traces out a periodic signature. When performing change detection analysis, we typically look for a sudden change in the signature, such as, sudden pronounced rise or drop in visual magnitude. Considerable guesswork is needed to infer what such a change might mean in terms of attitude changes. These plots were instrumental in detecting the stability of the Intelsat 33E post-fragmentation and the stability of all the fragments.

2.3 Pass schedule

A pass schedule is a useful tool to predict the next collection pass for a specific RSO. NorthStar's pass schedule implements different sensor's types, with their intrinsic geometry and visibility constraints. Knowing when the next collection opportunity arises following an IOD can help orbital analysts track the debris in a more reactive way. Fig. 8 shows the header of the pass schedule application.

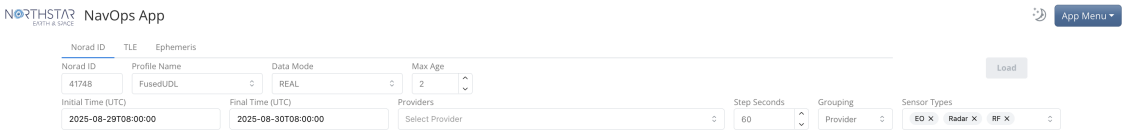

Fig. 8: Header of the Pass Schedule dashboard.

Copyright © 2025 Advanced Maui Optical and Space Surveillance Technologies Conference (AMOS) – www.amostech.com

3. SIMULATION RESULTS

This section will leverage the space-based observations simulated starting from SpaceTrack TLEs of the known debris objects as seen by NorthStar's constellation satellites to showcase the pipeline work and the NavOps tools. The outputs are shown in terms of: a single UCT manual handling, to highlight the steps and intermediate outputs, in Section 3.1; the pipeline overall breakup view to appreciate the fast spread of the debris, in Section 3.2.

3.1 Single UCT handling

We'll consider now simulated observations of Intelsat 33E debris NORAD ID 61988 for the remainder of this section. Fig. 9 shows the collection of observations during the first two days.

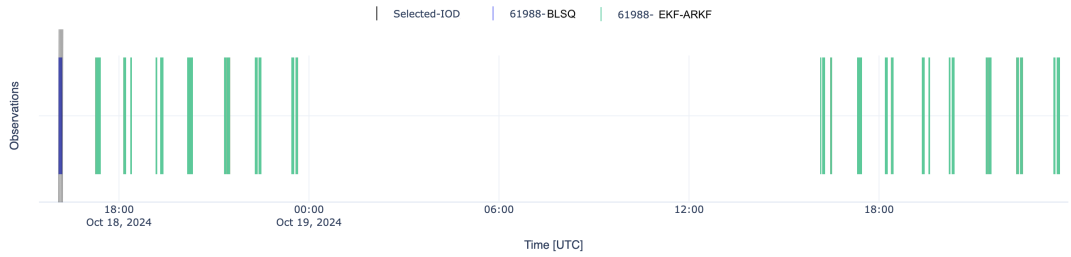

Fig. 9: Data collection for UCT 61988.

N-Gooding algorithm was applied to the first batch of observations on the first day of the breakup, as highlighted with the black lines in Fig. 9, resulting in an IOD solution, shown in the first column of Table 1. Only 8 minutes worth of observations were available resulting in a coarse initial guess.

Table 1: IOD initial state, BLSQ refinement, pipeline EKF

Semi-major axis (a)	43365.43 km	42309.01 km	42287.99 km
Eccentricity (e)	0.0271	0.006	0.006
Inclination (i)	0.25 deg	0.32 deg	0.32
RAAN (Ω)	141.39 deg	160.93 deg	159.63 deg
Argument of Perigee (ω)	157.66 deg	69.31 deg	66.91 deg

The IOD solve was then refined with a BLSQ on the same dataset, this time using all available observations, resulting in the second column of Table 1, corresponding to the blue stripes in Fig. 9, and with residuals shown in Fig. 10. One can appreciate the large variation in the orbit estimate after the BLSQ process and the struggle for BLSQ to converge.

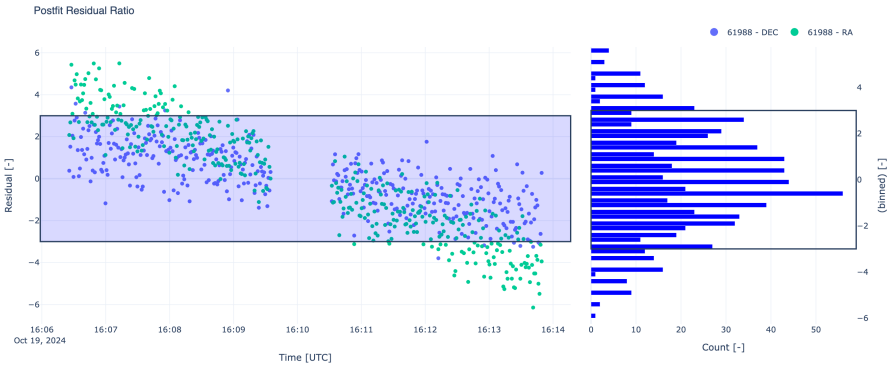

Fig. 10: Residual plot following a BLSQ.

During the following hours and days, the solution was sequentially refined by the pipeline with an EKF. Fig. 11 shows the sequential refinement of the solve: starting from the BLSQ solution - in blue, both filter had a large variation to

Copyright © 2025 Advanced Maui Optical and Space Surveillance Technologies Conference (AMOS) – www.amostech.com

adapt the solve to the new incoming observations. As expected, ARKF took noticeably less to reach convergence, while EKF took longer to stabilise. The converged solution is shown in the third column of Table 1 This was a case where manual intervention was not necessary, as, despite the initially inaccurate solve, custody of the object was never lost. Whenever smaller and/or fainter debris were observed on shorter arcs and less frequently, manual intervention was necessary either as explained in Section 2.1.3 or with a brand new IOD to recover the convergence of the solution.

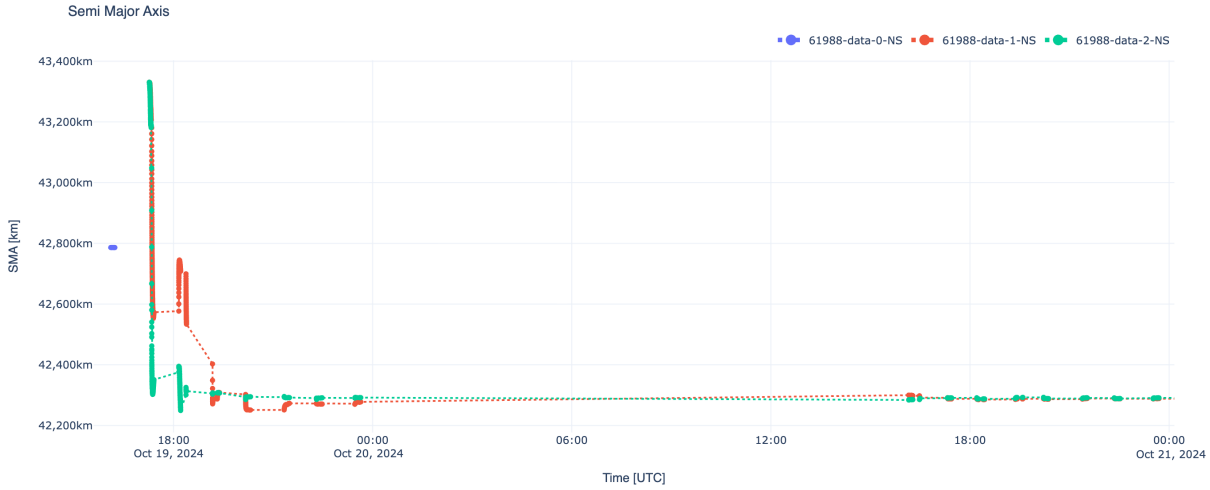

Fig. 11: Semi-major axis (SMA) evolution over time with BLSQ, EKF and ARKF filters.

In fact, the BLSQ step was found to be the most valuable step to obtain accurate solutions that could still be autonomously processed by the pipeline despite the large gaps in observations. The breakup time could then be estimated by back-propagating the well-characterised UCT to find the time of closest approach with the parent object INTELSAT 33E. While the waterfall plot in Fig. 14 allows for some coarse estimate, the use of CAS allowed for a more accurate breakup time estimation, as shown in Fig. 6, where the latest available TLE of Intelsat 33E is propagated forward and the first TLE of Intelsat 33E debris NORAD ID 61988 is propagated back-wards to obtain the relative geometry, TCA and DCA (which is not exactly zero due to the uncertainty involved).

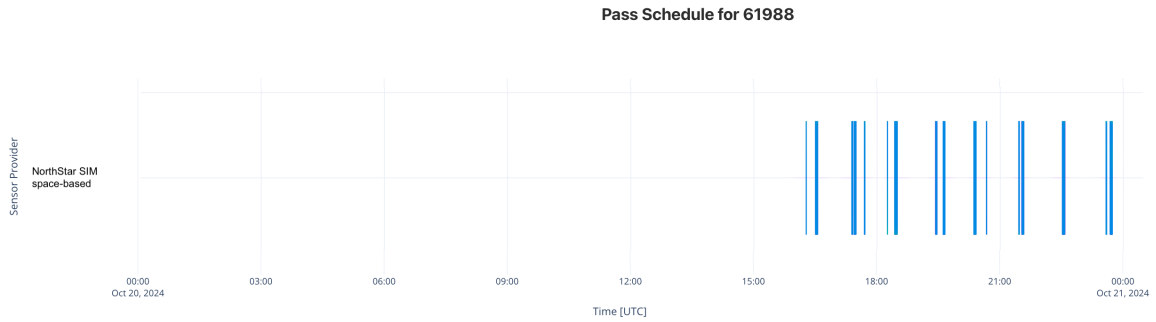

Fig. 12: Pass schedule for UCT 61988.

Lastly, collection opportunities for the UCT were obtained through the pass schedule, as shown in Fig. 12 where the latest available solve was used to predict the next passes through available sensors.

Copyright © 2025 Advanced Maui Optical and Space Surveillance Technologies Conference (AMOS) – www.amostech.com

3.2 Daily Operations on the Fragmentation Event

NorthStar constantly monitored and reported the fragmentation event daily during the initial monitoring days to assess the effects on the GEO belt. Twice a day, NorthStar generated a list of all the catalogued debris in the form of TLEs, together with a COMBO assessment to identify possible threats to neighbouring RSOs. Other products aided in the debris visualisation cloud spread and goodness of the ODs. These included the waterfall plot to assess the spread of fragments in the GEO belt and orbit plots (here shown in Fig. 13 with SpaceTrack data).

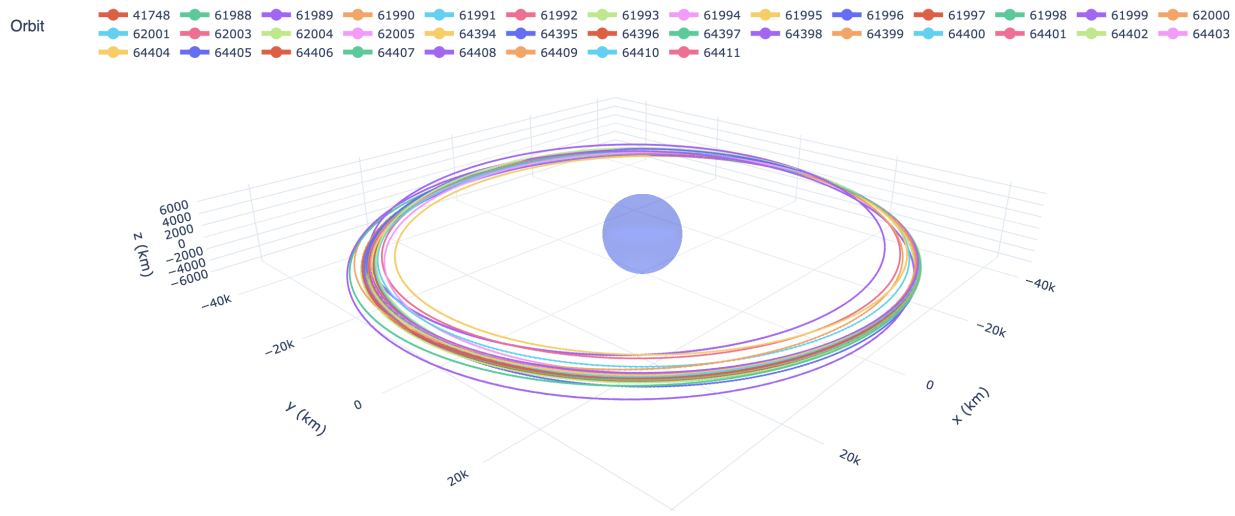

Fig. 13: Debris orbits generated with SpaceTrack data.

Daily reporting involved using the updated states for each fragment and ingesting data for any new fragments tracked to generate complete situational awareness of the event.

3.2.1 Waterfall

The time-based longitudinal information from the updated states of the UCTs associated with the breakup objects allows us to visualise the fragmentation resulting from the breakup, and can be used to understand the impact on the GEO belt by the longitudinal spread of the breakup fragments. Fig. 14 shows an example generated with SpaceTrack data. It is apparent from the spread of these objects over the longitudes that the GEO belt was entirely covered within a few days of the breakup, emphasising the risk and dangers of such events and stressing the need for accurate conjunction assessment.

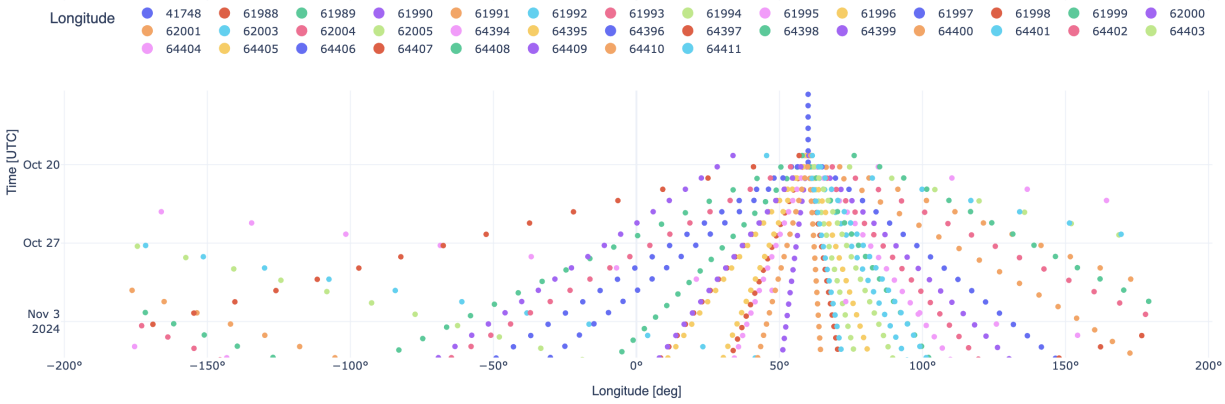

Fig. 14: Waterfall plot generated with SpaceTrack data.

Copyright © 2025 Advanced Maui Optical and Space Surveillance Technologies Conference (AMOS) – www.amostech.com

4. CONCLUSIONS

Using the Intelsat 33E breakup event, this document showcased NorthStar's automated pipeline, demonstrating both cataloguing and maintenance capabilities which enable operational tools for situational awareness. The results were shown by simulating space-based observations of Intelsat 33E debris with NORAD ID 61988. The fragmentation event was key in testing NorthStar's innovative IOD pipeline which had been deployed a few days earlier. The pipeline deployment aided in the success of the UCT handling, otherwise the number of fragment analyses needed would have made this task impossible with manual intervention. It also uncovered criticalities in handling borderline VSA tracks with predefined parameters, which made the team intervention necessary to ensure a successful IOD and OD on the fragments. The comprehensive situational awareness for the event was also developed using several NorthStar operations tools, such as, neighbourhood tables, photometry, waterfall, pass schedule etc. These tools enabled the correct identification of the breakup object, proper tracking of all the fragments, coverage of the neighbourhood of the fragments, and an elaborate conjunction assessment against the entire catalog. This was essential in developing a threat assessment of the complete GEO belt. The event has shaped NorthStar road maps to improve our automated cataloguing efforts to be able to handle such events and keep an accurate catalogue to ensure a safe utilisation of space.

REFERENCES

[1] Intelsat 33e (norad 41748). Satellite database entry, 2016. Geostationary satellite launched 24 August 2016 (COSPAR 2016-053B), Intelsat operator, BSS-702 MP bus, in geostationary orbit.

[2] European Space Agency – Space Debris Office. Intelsat-33e fragmentation. Blog post on ESA's fragmentation database, 2025. Analysis of the breakup and debris from the Intelsat 33e satellite.

[3] Intelsat. Intelsat reports IS-33e satellite loss. Press release, October 2024. Anomaly on October 19 led to total loss of the Intelsat 33e satellite; Intelsat is coordinating with Boeing and government agencies.

[4] Renato Gomes Silva, José Henrique Fernandez, and Giuliani Paulineli Garbi. On geospace conditions during the intelsat-33e satellite fatal failure in october 2024. SSRN preprint, July 2025. 20 pages; describes how geomagnetic storm and elevated radiation conditions likely contributed to the Intelsat-33e breakup.

[5] B. Golf and A. Konnath. Joint Commercial Operations (JCO) Introduction and Way Forward. In *Proceedings of the Advanced Maui Optical and Space Surveillance Technologies Conference (AMOS 2024), Wailea, HI*, 2024.

[6] G. Gerber, G. Badura, J. Bell, K. White, and S. Kharabash. Joint Commercial Operations (JCO) – Integrated Space Operations with Event Ledgers. In *Proceedings of the Advanced Maui Optical and Space Surveillance Technologies Conference (AMOS 2024), Wailea, HI*, 2024.

[7] Laura Pirovano, Daniele Antonio Santeramo, Roberto Armellin, Pierluigi di Lizia, and Alexander Wittig. Probabilistic data association based on intersection of Orbit Sets. In *Proceedings of the 19th AMOS Conference, September 11-14, 2018, Maui, USA*. Maui Economic Development Board, Inc., 2018.

[8] Maisonobe, Bryan Cazabonne, Evan Ward, Romain Serra, Maxime Journot, Sébastien Dinot, Guilhem Bonnefille, Thomas Neidhart, Luc Maisonobe, Clément Jonglez, Mark Rutten, yjeand, Julio Hernanz, lirw1984, Vincent Cucchietti, Andrew Goetz, Guiuux, gaetanpierre0, Lars Næsbye Christensen, Alberto Fossà, jvalet, Alberto Ferrero, gabb5, liscju, Christopher Schank, Tanner Mills, plan3d, Vyom Yadav, Shiva Iyer, and Petrus Hyvönen. Cs-si/orekit: 12.2, October 2024.

[9] C.H. Acton. Ancillary data services of nasa's navigation and ancillary information facility. *Planetary and Space Science*, 44:65–70, 1996.

[10] Space-track.org. `https://www.space-track.org/`. Accessed: 2025-08-29.

[11] R. R. Karimi and Daniele Mortari. Initial orbit determination using multiple observations. *Celestial Mechanics and Dynamical Astronomy*, 109:167–180, 2011.

[12] Byron D. Tapley, Beverly W. Schutz, and George H. Born. *Statistical Orbit Determination*. Elsevier Academic Press, Burlington, MA, 1st edition, 2004.

[13] Yuanxi Yang. Adaptively robust kalman filters with applications in navigation. In Guochang Xu, editor, *Sciences of Geodesy – I*, chapter 2, pages 19–58. Springer, 2010.

[14] John L. Africano, Paul Kervin, Doyle Hall, Paul Sydney, John Ross, Tamara Payne, Steve Gregory, Kira Jorgensen, Kandy Jarvis, Tracy Parr-Thumm, Gene Stansbery, and Ed Barker. Understanding photometric phase angle corrections. In *Proceedings of the Fourth European Conference on Space Debris*, ESA SP-587, pages 1–6, Darmstadt, Germany, April 2005. European Space Agency. Paper presented at the ECSD, April 18–20, 2005.

Copyright © 2025 Advanced Maui Optical and Space Surveillance Technologies Conference (AMOS) – www.amostech.com